DOI: 10.1002/ejic.200700390

Facile Synthesis and Photoluminescence of Europium Ion Doped LaF_3 Nanodisks

Ling Zhu,[a,b] Jian Meng,[a] and Xueqiang Cao*[a]

Keywords: Materials science / Crystal growth / Rare earths / Fluorescence

LaF_3:Eu^{3+} (5.0 mol-% Eu^{3+}) nanodisks with perfect crystallinity were successfully synthesized by a simple method. The synthesis was carried out in an aqueous solution at room temperature without the use of templates or organic additives. The mechanism of formation of the nanodisks was explored, and the fluoride source (KBF_4) is believed to play a key role in controlling the morphology of the final product. Furthermore, the size of the disk can be simply moderated by varying the concentration of the initial reactants. The room-temperature photoluminescence of LaF_3:Eu^{3+} with different morphologies and sizes were also investigated, and the results indicate that the emission intensity of the product is strongly affected by their size, shape, and other factors.

Introduction

Inorganic materials with controllable morphologies and sizes have attracted increasing attention because of their unique morphology- and size-dependent chemical and physical properties.[1–5] To date, a number of synthetic approaches including laser ablation, templating direction, electrochemical deposition, thermolysis of complex precursors in solution phase, and solvothermal/hydrothermal treatments have been developed to control the morphologies of materials.[6–11] However, the reported conventional methods suffer from the requirement of a template, high temperatures, special conditions, or tedious procedures, and therefore, facile and template-free methods are highly desired. Because of the significant advantages, such as the ease of control, low temperature, low cost, and easy scale-up, the stirring method is a powerful and practical route to prepare a great deal of inorganic materials with uniform and unique morphologies. Recently, great progress was made in the synthesis of nanodisks. Wu et al. reported the preparation of monodispersive silver nanodisks by thermolysis of the layered silver thiolate precursor.[12] Zhang et al. successfully synthesized ultrathin WO_3 nanodisks by using a wet chemical route with polyethylene glycol (PEG) as the surface modulator.[13] Korgel et al. developed the solvent-free thermolysis of a copper alkylthiolate molecular precursor to prepare Cu_2S nanodisks.[14] Iron oxide nanodisks can also be obtained through the nonhydrolytic, surfactant-mediated thermal reaction of iron pentacarbonyl and an oxidizer.[15] The growth of $Cd(OH)_2$ nanodisks by a hydrothermal route was reported by Zhang et al.[16]

The study of rare-earth fluorides is currently an active research field in modern materials chemistry as these compounds have potential applications in optics, optoelectronics, biological labeling, catalysis fields, etc.[17–21] Rare-earth fluoride crystals with various morphologies have been prepared by different synthetic techniques, for example, fullerene-like LnF_3 (Ln = La, Pr, Nd, Sm, and Y),[22,23] bundle-like, rod-like, hexagonal and triangular YF_3 nanocrystals,[24–26] monodisperse LaF_3 triangular nanoplates,[27] and EuF_3 nanocrystals with different crystalline phases and morphologies.[28,29] Wang et al. reported a hydrothermal method for the growth of LaF_3 nanodisks using $KF{\cdot}2H_2O$ as the fluoride source, and then the self-assembly of these nanodisks into the plate-built cylinders through oriented aggregation.[30] However, it is still a challenge to develop a more simple method to prepare LaF_3:Eu^{3+} with the controlled morphology under mild reaction conditions. Herein, we report a facile and fast solution-based method for the synthesis of singly crystalline LaF_3:Eu^{3+} nanodisks without the use of templates or organic additives, and further investigate their microstructure and luminescence properties.

Results and Discussion

Structure and Morphology of the Product

The crystal structure of the LaF_3:Eu^{3+} sample was characterized by XRD. As shown in Figure 1, all the peaks can be readily indexed to a hexagonal structure of LaF_3 [space

[a] Key Laboratory of Rare Earth Chemistry & Physics, Changchun Institute of Applied Chemistry, Chinese Academy of Sciences
Changchun, 130022 Jilin, China
Fax: +86-431-85262285
E-mail: xcao@ciac.jl.cn,
[b] Graduate School of the Chinese Academy of Sciences
Beijing 100049, China

group $P\bar{3}c1$ (No. 165)] with lattice constants of a = 7.187 Å and c = 7.350 Å (JCPDS No. 32–0483). No impurities were observed in the XRD pattern. The strong and sharp diffraction peaks indicate that the product crystallizes well.

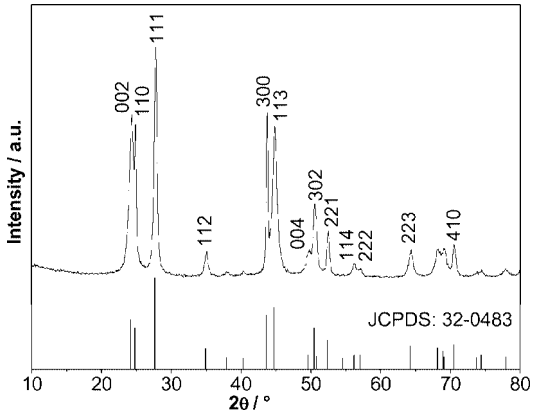

Figure 1. XRD pattern of the LaF_3:Eu^{3+} nanodisks.

The morphology and microstructure detail of the as-synthesized sample was investigated by SEM, TEM, HRTEM, and SAED observation. The SEM image with a low magnification (Figure 2a) reveals that the LaF_3:Eu^{3+} product is entirely comprised of disks with a uniform size and round shape. The average diameter of the disks is about 500 nm, as can be seen from the SEM with a high magnification (Figure 2b), and this is confirmed by the TEM images (Figure 2c). The thickness of the disk is about 20 nm, as observed from those disks that are perpendicular to the silicon substrate in the SEM image (Figure 2b). Furthermore, Figure 2b shows that the surfaces of the LaF_3:Eu^{3+} nanodisks are extremely smooth. The clear lattice fringes in the HRTEM image (Figure 2d) confirm the high crystallinity of the LaF_3:Eu^{3+} nanocrystals. The SAED image (Figure 2e) of a disk shows the regular diffraction spots and confirms that the LaF_3:Eu^{3+} nanodisks are singly crystalline. Furthermore, the diffraction observation indicates that <1120> is the growth direction for developing the hexagonal crystals, and the LaF_3:Eu^{3+} nanodisks are dominated by {0001} facets. These results indicate that LaF_3:Eu^{3+} nanodisks with uniform morphology and size can be obtained by this simple and mild method, and the productivity of the product is as high as 81%.

It is well-known that lanthanum fluoride has a small solubility product constant (K_{sp} = 2.0×10^{-19} at 25 °C),[31] implying that upon direct mixing, La^{3+} and F^- would immediately react to form the precipitate of lanthanum fluoride. For this rapid reaction it is thus difficult to control the morphology and size of the product. Figure 3 show the TEM images of the LaF_3:Eu^{3+} samples that were synthesized by using either NaF or NH_4F as the fluoride source, and the other preparation conditions are identical to those of the disk-like product. It can be seen that the LaF_3:Eu^{3+} samples are composed of irregular nanoparticles with serious agglomeration (Figure 3). Moreover, the SAED images of these two samples reveal that the LaF_3:Eu^{3+} nanoparticles are polycrystalline in nature (insets of Figure 3). In the case

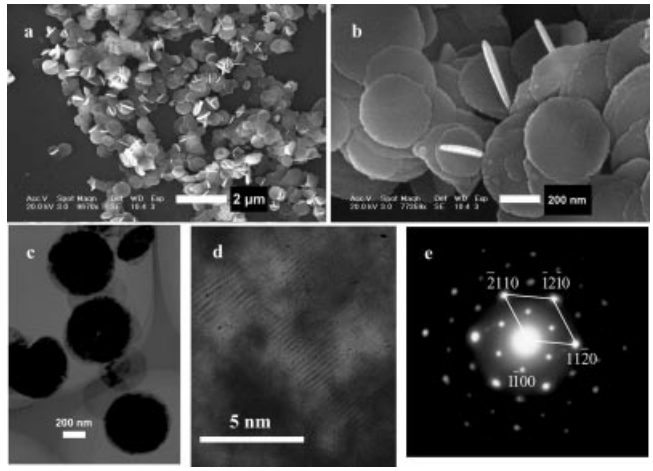

Figure 2. SEM images of the LaF_3:Eu^{3+} nanodisks with different magnification (a, b), TEM (c), HRTEM (d), and SAED (e) images of the LaF_3:Eu^{3+} nanodisks.

of NaF and NH_4F, a white precipitate appeared immediately after the lanthanum nitrate solution was mixed with sodium or ammonium fluoride, which indicated that the nucleation had taken place rapidly. These results indicate that in the current case, the rapid reaction process is not suitable to prepare LaF_3:Eu^{3+} with controlled morphology and size. Therefore, to solve these problems, a slow reaction process was adopted. It is interesting to observe that the experimental phenomena and the morphology of the final product are different when KBF_4 is used as the fluoride source. When KBF_4 was used, the reaction solution became turbid after 40 min, and the uniform nanodisks were formed. In an aqueous solution, KBF_4 was slowly hydrolyzed to produce F^- anions; these F^- anions reacted with Ln^{3+} cations (Ln = La, Eu) to form the lanthanum fluoride as described by Equations (1) and (2).

$$BF_4^- + 3H_2O \leftrightarrow H_3BO_3 + 3HF + F^- \quad (1)$$

$$Ln^{3+} + 3F^- \rightarrow LnF_3\downarrow \quad (2)$$

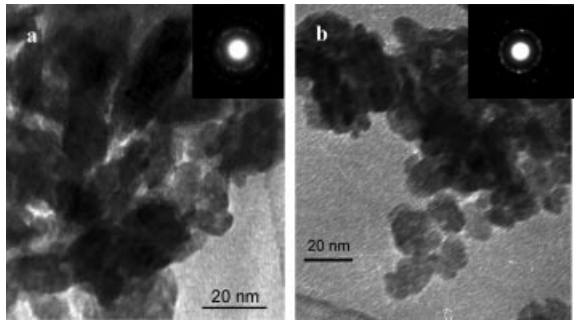

Figure 3. TEM (a) and SAED (inset a) images of the LaF_3:Eu^{3+} nanocrystal from NaF and the TEM (b) and SAED (inset b) images of the LaF_3:Eu^{3+} nanocrystal from NH_4F.

The equilibrium constant of the hydrolysis reaction [Equation (1)] is very small (K^0 = 6.41×10^{-12} at 25 °C)[32], which is helpful to keep the concentration of F^- ions in the reaction solution at a low level, and consequently, this leads

to slow crystallization of the product. The slow crystallization process can be further confirmed by the experimental observation that the reaction solution became turbid after stirring for 40 min, and the pH value of the aqueous solution gradually increased from approximately 5.0 at the beginning of the reaction to 1.5 when the reaction was complete. From the above observation, it is believed that the slow reaction process is a key factor for the synthesis of the singly crystalline $LaF_3:Eu^{3+}$ nanodisks with uniform morphology and size. Mann et al. reported the synthesis of Prussian blue nanoparticles and nanocrystal superlattices by the slow photoreduction of $[Fe(C_2O_4)_3]^{3-}$ to Fe^{2+} in the presence of $[Fe(CN)_6]^{3-}$ in reverse microemulsion.[33] Hu et al. synthesized perfect α-Fe_2O_3 fractal dendrites by the slow decomposition and hydrolysis of $K_3Fe(CN)_6$ under hydrothermal conditions.[34] Therefore, it can be reasonably inferred that a slow reaction process is very useful to control the morphology and size of the materials, especially for those with small K_{sp} values.

A crystal growth process consists of the nucleation and the growth, which are affected by the intrinsic crystal structure and the external conditions such as the kinetic energy barrier, temperature, time, and capping molecules, etc. Generally speaking, for materials with a hexagonal structure, the anisotropic growth along the *c* axis is available to form the 1D nanostructures, as the {001} planes (which are perpendicular to the *c* axis) exhibit significantly different surface energies relative to the {100} and {110} crystal planes. However, in the current case, only nanoparticles were obtained when NaF or NH_4F was used as the fluoride source and 2D nanodisks were obtained if KBF_4 was used as the fluoride source, indicating that KBF_4 plays a critical role in the formation of 2D nanodisks of the $LaF_3:Eu^{3+}$ crystals. BO_3^{3-} ions are produced during the hydrolysis of KBF_4 in aqueous solution as shown in Equation (1), and their appearance has been proven by other groups.[35] It is quite possible that these anions, such as BF_4^-, NO_3^-, and BO_3^{3-}, are adsorbed on the (0001) plane of the crystal seed, which slow down the crystal growth along the <0001> orientation. Accordingly, the intrinsically anisotropic growth of LaF_3 along the <0001> direction is substantially suppressed, and the 2D disk-like LaF_3 is formed. It is well-documented that adsorbed ions can change the growth kinetics and the surface energies of different crystal faces, which can ultimately lead to anisotropic growth of low-symmetry nanostructures, such as the nanodisk, the nanoplate, the nanorod, and the nanowire.[36–39] For example, Liu et al. used a seed growth procedure to obtain a complex hexagonal ZnO nanostructure with capping of the citric acid, which adsorbs preferably on the (001) surface of ZnO and slows down the crystal growth along the *c* axis.[40] Xia et al. observed that the polyvinylpyrrolidone capping agent interacted more strongly with the silver atoms on the {100} facets than those on the {111} facets, and the growth of silver could be directed into a highly anisotropic mode to form uniform nanowires.[41] Accordingly, in this work, KBF_4 is believed to play a key role in the formation of $LaF_3:Eu^{3+}$ nanodisks in the adopted reaction system. Therefore, through the above analysis, it is proposed that there are two key factors that allow $LaF_3:Eu^{3+}$ nanocrystals with the 2D disk-like morphology to be obtained. One is the slow reaction process, and the other is the selective absorption of anions (BF_4^-, NO_3^-, BO_3^{3-}) specifically on the crystal faces of the crystal seed. However, the mechanism of formation of the $LaF_3:Eu^{3+}$ nanodisks is not fully understood. Further theoretical and experimental work is required to understand the exact nature of the mechanism of growth.

Further experiments indicated that the size of the synthesized $LaF_3:Eu^{3+}$ disk depends strongly on the concentration of the initial reagents. At the fixed molar ratio of 3:1 for KBF_4:La(Eu)$(NO_3)_3$, the size of the product decreased from 500 to 100 nm with an increase in the initial concentration of the reactant. Figure 4a shows a typical SEM image of a $LaF_3:Eu^{3+}$ sample that was prepared from an aqueous solution in which the concentrations of La(Eu)$(NO_3)_3$ and KBF_4 were 0.04 and 0.12 M, respectively. The average size of the disk is 300 nm. A further increase in the concentration of La(Eu)$(NO_3)_3$ to 0.08 M and that of KBF_4 to 0.24 M caused the average size of the disk to be reduced to 100 nm, as illustrated in Figure 4b. Moreover, it is obvious that the surface of the nanodisk becomes coarse with an increase in the concentration of the initial reagents. The above experiments indicate that the size of the $LaF_3:Eu^{3+}$ disks could be tuned by simply changing the concentrations of the precursors.

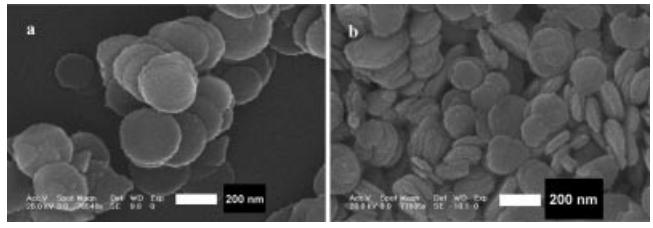

Figure 4. SEM image (a) of the $LaF_3:Eu^{3+}$ nanocrystal with La(Eu)$(NO_3)_3$ and KBF_4 concentrations of 0.04 and 0.12 M, respectively, and the SEM image (b) of the $LaF_3:Eu^{3+}$ nanocrystal with La(Eu)$(NO_3)_3$ and KBF_4 concentrations of 0.08 and 0.24 M, respectively.

Photoluminescent (PL) Properties

Figure 5 shows the room-temperature emission spectra of $LaF_3:Eu^{3+}$ nanodisks and nanoparticles that were prepared from different fluoride sources. Both samples were measured under identical conditions with an excitation wavelength of λ_{ex} = 399 nm. In the emission spectra, the characteristic emission peaks of Eu^{3+} in the wavelength range from 520 to 720 nm were observed, corresponding to the transitions from the excited $^5D_1$ and $^5D_0$ levels to ^7F_J (J = 0–4) levels, with the magnetic dipole $^5D_0 \rightarrow {}^7F_1$ allowed transition (589 nm) being the most prominent emission line.[42] The relative intensities of the emission peaks were similar to those reported earlier,[19] indicating that the Eu^{3+} ion is located in the La^{3+} crystal site with C_2 symmetry,

which is the same as that of the bulk LaF_3 crystals.[43] For the C2 site, the electric and magnetic dipole transitions are allowed. Therefore, both the $^5D_0 \rightarrow {}^7F_1$ and the $^5D_0 \rightarrow {}^7F_2$ transitions of Eu^{3+} can be observed in the LaF_3:Eu^{3+} nanocrystals. Although the emission positions of the major peaks of these two samples are identical, the emission intensity of the disk-like LaF_3:Eu^{3+} product is significantly higher than that of the particle-like product. It is well-documented that the grain size, morphology, crystal structure, dimension, and surface modification of the luminescent material all influence its photoluminescent properties.[44–46] Owing to a large surface area to volume ratio, an important source of luminescence quenching in small particles is the surface where the coordination of the atom differs from that in the bulk and the site where different chemical species can be adsorbed. Because the samples were prepared in aqueous solution, the surface of the nanocrystals can be covered with hydroxy species such as lanthanum or europium hydroxides, fluorine ions, or adsorbed water molecules. Different sizes and shapes result in different combinations between the surface and the adsorbed species so as to produce different quenching abilities of the emissions of the Eu^{3+} ions; therefore, the differences in the PL intensities of the samples may be attributed to the different abilities of the adsorbed species on the surface to quench the emissions from the Eu^{3+} ions. The luminescence intensity of the disk-like nanocrystals is obviously stronger than that of the particle-like nanocrystals, which may be due to the factor that the nanostructure can prevent the adsorbed species on the surface from quenching the emission from the Eu^{3+} ions. We also assume that the particle-like crystals would possess more defects due to the fast growth of the crystal. Some of these defects may act as the nonradiative recombination centers, and they may be responsible for the decrease in the luminescence intensity as observed in the particle-like product.

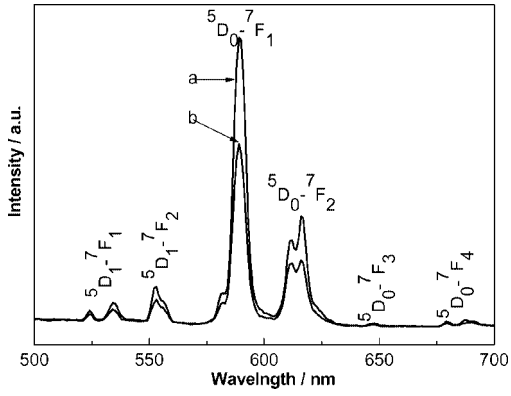

Figure 5. Emission spectra of the nanodisks (a) and nanoparticles (b) of LaF_3:Eu^{3+} nanocrystals.

The emission spectra of LaF_3:Eu^{3+} disks with different sizes under excitation at 399 nm were also investigated. From Figure 6 it can be seen that the emission intensity of the LaF_3:Eu^{3+} phosphors basically increase with an increase in the size of the disks. It is well-known that a large particle size is helpful for improving the PL intensity of phosphors.[47,48] A more extensive investigation of the differences in the luminescent properties of the products with different morphologies, crystal structures, sizes, and dimensions will be further investigated in our future work.

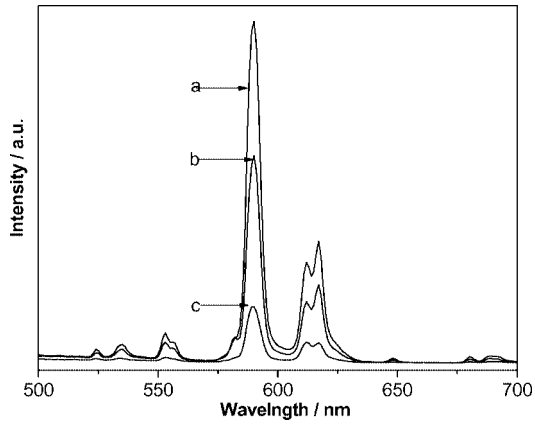

Figure 6. Emission spectra of the LaF_3:Eu^{3+} disks with different size: 500 nm (a), 300 nm (b), and 100 nm (c).

Conclusions

We utilized a mild and facile synthetic route to prepare LaF_3:Eu^{3+} nanodisks from an aqueous solution of $(La,Eu)(NO_3)_3$ and KBF_4 without the use of templates or organic additives. The size of the LaF_3:Eu^{3+} nanodisks can be tuned by simply controlling the concentration of the precursors. The mechanism of formation of the disk-like structures was investigated, and the fluoride source (KBF_4) clearly contributes to the creation of such a structure. Room-temperature photoluminescence of the LaF_3:Eu^{3+} samples with different morphologies and sizes were also investigated, and the results reveal that all of these samples showed similar features but different luminescence intensities.

Experimental Section

General: All the reagents used were of analytical grade, including La_2O_3 and Eu_2O_3 (Shanghai Chemical Reagent), KBF_4, NaF, and NH_4F (Beijin Chemical Reagent), and used as received without further purification.

Typical Synthesis: Appropriate amounts of La_2O_3 and Eu_2O_3 (La:Eu = 95:5, in molar ratio) were first dissolved in nitric acid (10%) and then mixed with a KBF_4 solution in a 150-mL plastic flask to give a final concentration of 20 mM of $La(Eu)(NO_3)_3$ and 60 mM of KBF_4. The total volume of the solution was 100 mL. The resulted solution was stirred at ambient temperature for 3 h. A white precipitate was centrifuged and then washed with distilled water and absolute ethanol in sequence. The final product was dried under vacuum at 60 °C for 12 h.

Crystal Structure Determination: X-ray powder diffraction (XRD) was performed with a Rigaku D/MAX-2500 diffractometer with Cu-K_α radiation (λ = 0.15406 nm) and a scanning rate of 5 °min^{-1}.

Scanning electron micrographs (SEM) were taken with a XL30 field-emission scanning electron microscope. Transmission electron micrographs (TEM), high-resolution transmission electron micrographs (HRTEM), and the selected area electron diffraction (SAED) were taken with a JEOL-JEM-2010, operating at 200 kV (JEOL, Japan). Samples for TEM were prepared by dropping a diluted suspension of the sample powders onto a standard carbon-coated (20–30 nm) Formvar film on a copper grid (230 mesh). Photoluminescence (PL) spectra were recorded with a Hitachi F-4500 spectrophotometer equipped with a 150 W xenon lamp as the excitation source. All the measurements were performed at room temperature.

Acknowledgments

This work was financially supported by the National Nature Science Foundation of China (No. 20331030).

[1] M. Pal, J. G. Serrano, P. Santiago, U. Pal, *J. Phys. Chem. C* **2007**, *111*, 96–102.
[2] Y. F. Hao, G. W. Meng, C. H. Ye, L. D. Zhang, *Cryst. Growth Des.* **2005**, *5*, 1617–1621.
[3] J. Geng, Y. N. Lv, D. J. Lu, J. J. Zhu, *Nanotechnology* **2006**, *17*, 2614–2620.
[4] T. Xia, Q. Li, X. D. Liu, J. Meng, X. Q. Cao, *J. Phys. Chem. B* **2006**, *110*, 2006–2012.
[5] A. Miyazaki, I. Balint, Y. Nakano, *J. Nanopart. Res.* **2003**, *5*, 69–80.
[6] J. Q. Hu, Q. Li, X. M. Meng, C. S. Lee, S. T. Lee, *J. Phys. Chem. B* **2002**, *106*, 9536–9539.
[7] Z. F. Pu, M. H. Cao, J. Yang, K. L. Huang, C. W. Hu, *Nanotechnology* **2006**, *17*, 799–804.
[8] B. Q. Cao, Y. Li, G. T. Duan, W. P. Cai, *Cryst. Growth Des.* **2006**, *6*, 1091–1095.
[9] P. Gao, Y. Xie, L. N. Ye, Y. Chen, Q. X. Guo, *Cryst. Growth Des.* **2006**, *6*, 583–587.
[10] Z. A. Peng, X. G. Peng, *J. Am. Chem. Soc.* **2001**, *123*, 1389–1395.
[11] H. S. Qian, S. H. Yu, J. Y. Gong, L. B. Luo, L. L. Wen, *Cryst. Growth Des.* **2005**, *5*, 935–939.
[12] Y. B. Chen, L. Chen, L. M. Wu, *Inorg. Chem.* **2005**, *44*, 9817–9822.
[13] A. Wolcott, T. R. Kuykendall, W. Chen, S. W. Chen, J. Z. Zhang, *J. Phys. Chem. B* **2006**, *110*, 25288–25296.
[14] M. B. Sigman, J. A. Ghezelbash, T. Hanrath, A. E. Saunders, F. Lee, B. A. Korgel, *J. Am. Chem. Soc.* **2003**, *125*, 16050–16057.
[15] M. F. Casula, Y. W. Jun, D. J. Zaziski, E. M. Chan, A. Corrias, A. P. Alivisatos, *J. Am. Chem. Soc.* **2006**, *128*, 1675–1682.
[16] W. D. Shi, C. Wang, H. S. Wang, H. J. Zhang, *Cryst. Growth Des.* **2006**, *6*, 915–918.
[17] J. W. Stouwdam, C. J. M. van Veggel Frank, *Langmuir* **2004**, *20*, 11763–11771.
[18] L. Y. Wang, Y. D. Li, *Nano Lett.* **2006**, *6*, 1645–1649.
[19] J. W. Stouwdam, C. J. M. van Veggel Frank, *Nano Lett.* **2002**, *2*, 733–737.
[20] S. Sivakumar, P. R. Diamente, C. J. M. van Veggel Frank, *Chem. Eur. J.* **2006**, *12*, 5878–5884.
[21] J. Z. Luo, H. L. Wan, *Appl. Catal. A* **1997**, *158*, 137–144.
[22] X. Wang, Y. D. Li, *Angew. Chem. Int. Ed.* **2003**, *42*, 3497–3500.
[23] X. Wang, Y. D. Li, *Chem. Eur. J.* **2003**, *9*, 5627–5635.
[24] R. X. Yan, Y. D. Li, *Adv. Funct. Mater.* **2005**, *15*, 763–770.
[25] X. Wang, J. Zhuang, Q. Peng, Y. D. Li, *Inorg. Chem.* **2006**, *45*, 6661–6665.
[26] J. L. Lemyre, A. M. Ritcey, *Chem. Mater.* **2005**, *17*, 3040–3043.
[27] Y. W. Zhang, X. Sun, R. Si, L. P. You, C. H. Yan, *J. Am. Chem. Soc.* **2005**, *127*, 3260–3261.
[28] M. Wang, Q. L. Huang, J. M. Hong, X. T. Chen, Z. L. Xue, *Cryst. Growth Des.* **2006**, *6*, 1972–1974.
[29] M. Wang, Q. L. Huang, J. M. Hong, X. T. Chen, Z. L. Xue, *Cryst. Growth Des.* **2006**, *6*, 2169–2173.
[30] Y. Cheng, Y. S. Wang, Y. H. Zheng, Y. Qin, *J. Phys. Chem. B* **2005**, *109*, 11548–11551.
[31] T. L. Brown, H. E. LeMay Jr, B. E. Bursten, *Chemistry – The Central Science*, 8th ed., Prentice-Hall International, INC, **2000**, p. 1023.
[32] W. J. Crooks III, W. D. Rhodes, *Use of Modeling for the Prevention of Solids Formation during Canyon Processing of Legacy Nuclear Materials*, Westinghouse Savannah River Company Aiken, SC 29808,WSRC-TR-2002–00462, **2003**, p. 7.
[33] S. Vaucher, M. Li, S. Mann, *Angew. Chem. Int. Ed.* **2000**, *39*, 1793–1796.
[34] M. H. Cao, T. F. Liu, S. Gao, G. B. Sun, X. L. Wu, C. W. Hu, Z. L. Wang, *Angew. Chem. Int. Ed.* **2005**, *44*, 4197–4201.
[35] Z. J. Miao, Z. M. Liu, K. L. Ding, B. X. Han, S. D. Miao, G. M. An, *Nanotechnology* **2007**, *18*, 125605.
[36] A. Filankembo, S. Giorgio, I. Lisiecki, M. P. Pileni, *J. Phys. Chem. B* **2003**, *107*, 7492–7500.
[37] S. H. Im, Y. T. Lee, B. Wiley, Y. N. Xia, *Angew. Chem. Int. Ed.* **2005**, *44*, 2154–2157.
[38] B. Wiley, Y. G. Sun, B. Mayers, Y. N. Xia, *Chem. Eur. J.* **2005**, *11*, 454–463.
[39] K. K. Caswell, C. M. Bender, C. J. Murphy, *Nano Lett.* **2003**, *3*, 667–669.
[40] Z. R. Tian, J. A. Voigt, J. Liu, B. Mckenzie, M. J. Mcdermott, *J. Am. Chem. Soc.* **2002**, *124*, 12954–12955.
[41] Y. G. Sun, Y. D. Yin, B. T. Mayers, T. Herricks, Y. N. Xia, *Chem. Mater.* **2002**, *14*, 4736–4745.
[42] F. Wang, Y. Zhang, X. P. Fan, M. Q. Wang, *J. Mater. Chem.* **2006**, *16*, 1031–1034.
[43] W. T. Carnall, G. L. Goodman, K. Rajnak, R. S. Rana, *J. Chem. Phys.* **1989**, *90*, 3443–3457.
[44] C. Burda, X. B. Chen, R. Narayanan, M. A. El-Sayed, *Chem. Rev.* **2005**, *105*, 1025–1102.
[45] L. M. Chen, Y. N. Liu, K. L. Huang, *Mater. Res. Bull.* **2006**, *41*, 158–166.
[46] G. S. Yi, H. C. Lu, S. Y. Zhao, Y. Ge, W. J. Yang, D. P. Chen, L. H. Guo, *Nano Lett.* **2004**, *4*, 2191–2196.
[47] M. Yu, H. Wang, C. K. Lin, G. Z. Li, J. Lin, *Nanotechnology* **2006**, *17*, 3245–3252.
[48] X. Jing, T. G. Ireland, C. Gibbons, D. J. Barber, J. Silver, A. Vecht, G. Fern, P. Trogwa, D. Morton, *J. Electrochem. Soc.* **1999**, *146*, 4654–4658.

Received: April 8, 2007
Published Online: June 29, 2007

